

3.5 SCCMS Projects

Development of machine learning-aided simulation methods for molecular liquids

Hayato SHIBA

*Information Technology Center, University of Tokyo
6-2-3 Kashiwa-no-ha, Kashiwa, Chiba 277-0882*

Thanks to the present status of the art where basic simulation methodology for parallel MD simulations is approaching its maturity, many open source packages are commonly available for usage on supercomputers. However, how to simulate long-time phenomena remains a long-standing unresolved issue in molecular dynamics simulations. It is difficult to perform numerical time integration over 10^{10} steps which corresponds to $10 \mu\text{s}$ in all-atom modeling. I am pursuing a methodology for realizing simulation that can allow computations on both large-scale and long-time. The key to realizing this is the efficient usage machine learning for capturing the dynamical paths in the phase space. For a class of glassy materials, it is recently found that static structure have the power to predict in which regions particles have a high tendency to move over a long time by means of deep learning in terms of the graph neural networks (GNNs) [1]. In FY 2021, after October, we have started to further extend the predictive power of GNN.

Firstly I confirmed that results of a previous study [1] can be fully reproduced, both quantitatively and qualitatively, by using the dataset provided by its authors. The system I consider is Kob-Andersen-type Lennard-Jones (KALJ) liquid, wherein two types of particles are enclosed in a box with different interaction parameters and particle radii to bypass crystallization.

In Fig. 1, predicted propensity map is compared with the ground data in which the parti-

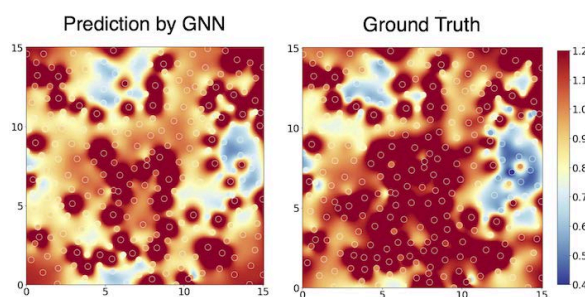


Figure 1: Color map indicating the predictive ability of particle propensity in KALJ liquid at a low temperature. where the 2D cross sections are shown here in the 3D system.

cle propensity is evaluated from direct molecular dynamics simulation. Further, I have extended the GNN learning model so that changeover in each neighbor pair distances can be learned as an edge feature on the GNN. As a result, the predictive ability has been extended into a wider temporal range, exceeding the propensity ability of the node feature (particle propensity) in Ref. [1] in the range from 10^3 to 10^8 MD steps. I have also clarified that predictive ability of the original model is decreased because of its inability to treat the collective motion induced by strain displacement.

Most of the resources allocated for my ISSP project in FY2021 are spent on extending the dataset to longer-time. I have extended the dataset to cover the time region up to $100\tau_\alpha$, where τ_α represents glassy relaxation time called α -relaxation time. As a large num-

ber of simulation snapshot is required for learning, the dataset is, in fact, very large. By providing 32 different random initial velocities 500 independent initial particle configurations which are fully relaxed at a target temperature of consideration, I have conducted 16,000 simulation in total of 3D KALJ liquids with 4,096 particles by my in-house simulation code. As a result, I have successfully revealed that the GNN begins to lose its predictive ability at the time scale close to τ_α . All the above results mentioned will be soon submitted as an original paper [2]. In association with this work, we have conducted machine learning performance evaluation by using the same model on NVIDIA A100 GPUs, wherein the evaluation itself is performed on Wisteria/BDEC-01 supercomputer at ITC, Univ. of Tokyo [3].

Further, I have analyzed the internal structure of the code and rewritten it in full for PyTorch Geometric (PyG) code which is a library for training on GNNs on PyTorch, while all the original code written for TensorFlow and JAX is distributed by the authors of Ref. [1]. This PyTorch extension will enable the community to further combine these prediction methods with existing tools used in molecular simulations, because PyTorch has now become the most popular frameworks used in ML-aided molecular simulations. The PyG code will soon be made publicly available via our GitHub repository [4].

References

- [1] V. Bapst *et al.*: Nat. Phys. **16**, 448-454 (2020).
- [2] H. Shiba *et al.*: in preparation.
- [3] H. Shiba and T. Shimokawabe: IPSJ SIG Technical Report, Vol. 2020-HPC-183(22), 1-11 (2022) (in Japanese).
- [4] <https://github.com/h3-Open-BDEC/>

Finite temperature dependence of ab-initio Hamiltonians and its analysis for two-dimensional organic conductors Pd(dmit)₂ Salts

Kazuyoshi YOSHIMI¹, Takao TSUMURAYA², and Takahiro MISAWA³

¹*Institute for Solid State Physics, University of Tokyo, Kashiwa 277-8581, Japan*

²*Priority Organization for Innovation and Excellence, Kumamoto University,*

Kumamoto 860-8555, Japan

³*Beijing Academy of Quantum Information Sciences, Haidian District, Beijing 100193, China*

The molecular solids β' -X[Pd(dmit)₂]₂ (where X represents a cation) exhibit various phases such as an antiferromagnetic phase, a quantum spin liquid, and a charge-ordered phase depending on the choice of X [1]. Comprehensive analyses of band calculations and transfer integrals based on the extended Hückel method and first-principles calculations have been carried out, and quantitative evaluation of the electronic states has been successfully performed [2]. However, electron correlation effects are expected to play a major role in order to elucidate the origin of these phenomena. Therefore, a quantitative derivation of the effective interactions using the constrained Random Phase Approximation (cRPA) is necessary for clarifying the microscopic origin of the stability of the quantum spin liquid. Moreover, it has been reported that the temperature dependence of the transfer integral is large for these materials [3]. The effective interactions are expected to have a similar temperature dependence.

In this study [4,5], we used the program RESPACK [6], which can derive the effective Hamiltonian describing low-energy degrees of freedom based on band structures obtained by first-principles calculations, to derive an effective Hamiltonian for the crystal structures reported in Ref. [3]. As a result, the transfer integrals tend to increase with decreasing temperature, while the effective interactions tend to decrease. The ratio of the transfer integral to the effective interaction was found to be about 20% smaller than that at room temperature. We also analyzed the obtained effective Hamiltonians using the exact diagonalization method with the boundary condition average by $H\Phi$ [7]. We find that the spin correlation function varies with the temperature dependence of the effective model, and in particular, the antiferromagnetic order moment decreases at β' -EtMe₃Sb[Pd(dmit)₂]₂, where the emergence of the quantum spin liquid is reported experimentally.

The overall tendency of the compound

dependence of the antiferromagnet ordered moment is consistent with the available experimental results. Our results demonstrate that the comprehensive derivation of the effective Hamiltonian and its analysis is a powerful method for elucidating the microscopic origin of exotic quantum states found in organic materials. In future research, we plan to apply this method to other organic materials that exhibit exotic quantum phases.

References

- [1] R. Kato, Chem. Rev., 104, 5319–5346 (2004).
- [2] K. Kanoda and R. Kato, Annu. Rev. Condens. Matter, Phys. 2, 167 (2011).
- [3] K. Ueda, T. Tsumuraya and R. Kato, Crystals 8, 138(2018).
- [4] T. Misawa, K. Yoshimi, T. Tsumuraya, Phys. Rev. Research 2, 032072(R) (2020).
- [5] K. Yoshimi, T. Tsumuraya, T. Misawa, Phys. Rev. Research 3, 043224 (2021).
- [6] K. Nakamura, Y. Yoshimoto, Y. Nomura *et al.*, Comp. Phys. Comm. 261, 100781(2021).
- [7] M Kawamura, K Yoshimi, T Misawa *et al.*, Comp. Phys. Comm. 217, 180(2017).

Large-Scale GW/BSE electronic structure calculations for metal-organic hybrid materials

Takatoshi Fujita

*National Institutes for Quantum Science and Technology
Tokai-mura, Naka-gun, Ibaraki 319-1106*

Accurate calculations of electronic states are essential for computational studies of organic materials which are directed toward understanding of fundamental processes in organic electronic devices. We have recently developed the large-scale GW method based on the fragment molecular orbital method. The fragmentation approximation for the total polarization function and the Δ COHSEX approximation have been employed for efficient evaluations of GW quasiparticle energies from localized molecular orbitals. More recently, we have proposed the novel large-scale excited-state methods based on the FMO, exciton model, and GW/BSE with Tamm-Dancoff approximation (TDA). In this method, the excited-state Hamiltonian matrix elements at the GW/TDA-BSE level is calculated in the basis of fragment configuration state functions which describe intrafragment excitations or interfragment charge-transfer excitations. The excited-state Hamiltonian is then diagonalized to approximate the adiabatic excited states of an entire system. We have confirmed that for molecular clusters, the novel fragment-based GW/TDA-BSE can reasonably reproduce the excited states obtained from conventional GW/TDA-BSE method. Our developments enables the applications of GW/TDA-BSE method to large molecular assemblies, which will be useful for investigating charge separation in condensed phase.

Recently, we have demonstrated that the accuracy of the total polarization function can be

systematically improved by including the two-body correction terms. At the static COHSEX level, errors of less than 10 meV relative can be achieved for realistic molecular aggregates. However, residual errors of up to 100 meV are still present, originating from the Δ COHSEX approximation. In addition, we assessed the dependence of the total polarization function on the threshold distance and found that the convergence with respect to the threshold is slow. However, the threshold distance range of 1.5–2.0 nm was determined to be a reasonable compromise between the accuracy and computational effort, and the HOMO–LUMO gap and excitation energies reasonably reproduced in comparison with the results obtained without the cutoff. The present implementation offers a practical scheme for investigating large molecular systems. Applications to realistic molecular systems, such as organic light-emitting device materials and organic solar cells, are currently underway.

References

- [1] T. Fujita, Y. Noguchi, *J. Phys. Chem. A* **13** (2020) 2728.

Doping effects on P2 $\text{Na}_x\text{Mn}_{1-y}\text{M}_y\text{O}_2$ ($M=\text{Li, Mg, Al, Ti, V, Cr, Fe, Co, Ni}$) for sodium-ion rechargeable batteries: *Ab initio* investigations

Huu Duc LUONG^{1,2}, Hiroyoshi MOMIDA^{2,3}, Tamio OGUCHI^{2,3}

¹Graduate School of Engineering, Osaka University, Suita, Osaka 565-0871, Japan

²SANKEN, Osaka University, Ibaraki, Osaka 567-0047, Japan

³ESICB, Kyoto University, Kyoto 615-8245, Japan

P2 layered oxide Na_xMnO_2 exhibits a voltage window from 2.0 to 3.5V and high specific capacity up to 220mAh/g. However, the material suffers from the serious phase transformation during its charging/discharging.

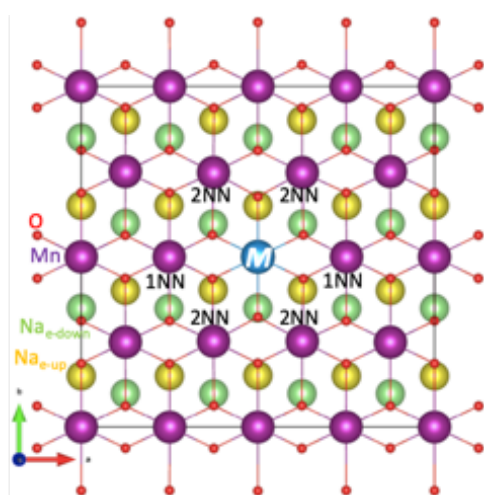


Fig. 1: Crystal structure of doped structure $\text{NaMn}_{1-y}\text{M}_y\text{O}_2$ ($y=0.0625$, $M = \text{Li, Mg, Al, Ti, V, Cr, Fe, Co, and Ni}$) along c -axis. Purple, red, blue, yellow and green balls illustrate Mn, O, M, upper-layered and lower-layered Na atoms. Surrounding each dopant, there are two nearest $\text{Mn}^{1\text{NN}}$ and four second nearest $\text{Mn}^{2\text{NN}}$ atoms.

Through the highly accurate hybrid functional method (HSE06), we computationally evaluate the doping influences on the lattice distortions, stabilities, electronic structures, redox potentials, and diffusion mechanisms [1]. The model for calculation is shown in Fig. 1. Our calculations indicate that dopants not only reduce the lattice distortion degree, especially for Li, Mg, Ti, and V cases, but also increase the stability of the structure, implying the dopants would alleviate the Jahn-Teller lattice distortion, as shown in Figs. 2(a) and 2(b). Figure 2(c) illustrates that at full Na concentrations, all the considered dopants, except for Ti and V, have a small effect on the redox potential. At low Na concentrations, the Li dopant preferably diffuses out of the MnO_2 layer, but hardly moves to the Na layer, suggesting that P2-layered oxides can prevent the dopant's migrations during the Na extractions due to the high relative energies.

The effect on the diffusion mechanism is described through the diffusion of a Na ion–

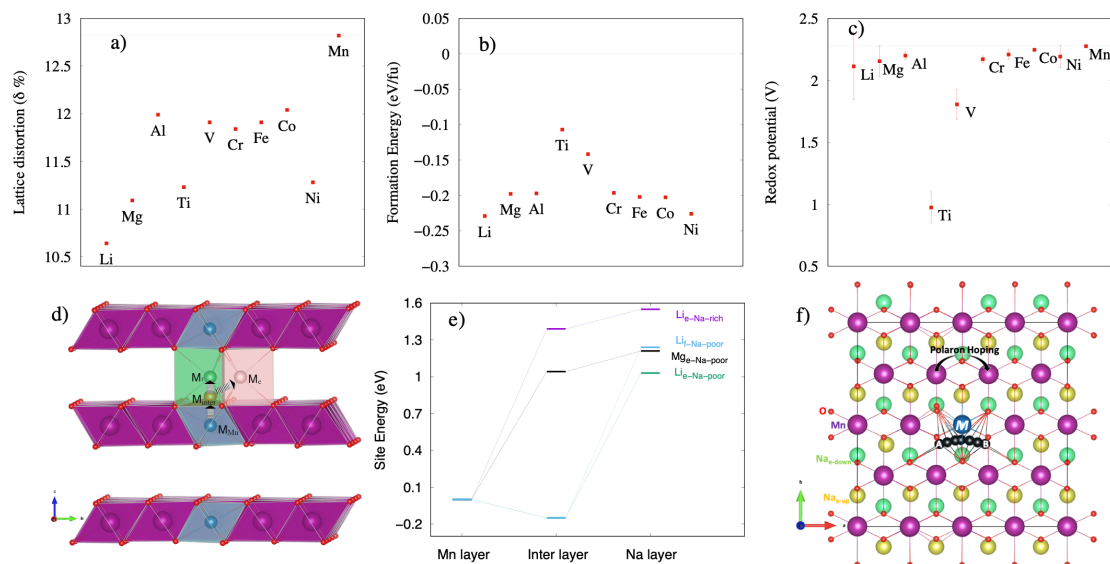


Fig. 2: a) Lattice distortion. b) Formation energy. c) Redox potential of NaMn_{1-y}M_yO₂. d) Dopant's migration path from Mn-layer site (blue balls) to intermediate site (brown balls) and to Na-layer face-shared sites (green balls) or edge-shared site (pink balls). e) Relative site energies of structures containing dopants at the Mn-layer site, intermediate site, edge-shared site and face-shared site in the Na-layer calculated along the dopant's migration paths ($M=Li, Mg$) at rich and poor Na contents. f) Diffusion path of a Na ion near the dopants. Green, yellow, red, purple, blue and black balls represent Na atoms at lower and upper layers, O, Mn, dopant M, and Na-vacancy trace. A and B stand for the initial and final position of Na ion for diffusion. An arrow indicates the polaron hopping between two adjacent Mn sites.

polaron complex near the dopant's environments, as shown in Fig. 2(f). Fe, Mg, Ti, and Cr dopants can hinder the Na ion-polaron complex diffusion with significantly higher activation energies, respectively, while the Al dopant almost remains the activation energy as well as the perfect structure. However, Li, V, Co, and Ni dopants benefit from such complex diffusion with much lower activation energy so the ion diffusivities

increase significantly. It is found that the doping influence on the activation energy for Na ion diffusion is associated with the $M-O$ bond change and charges of the neighboring dopants.

References

- [1] H. D. Luong, H. Momida, V. A. Dinh, T. Oguchi, Phys. Rev. Materials **6**, 015802 (2022).

Ab initio study toward abundant element nanocatalysts with less precious metals

Tetsuya TAKETSUGU

Faculty of Science, Hokkaido University

N10W8, Sapporo, Hokkaido 060-0810

DFT computations with QuantumEspresso (QE) are used to gain chemical insights and to design novel catalysts with abundant elements such as hexagonal boron-nitride (h-BN) for reducing costs and dependences on precious metals used in various heterogeneous catalysts.

We have elucidated the catalytic activity of oxygen functionalized hexagonal boron nitride (h-BN) with *B-O-O-B* and *B-O-B* active sites at the zigzag edges for oxidative dehydrogenation (ODH) of light alkanes, specifically ethane (C_2H_6), propane (C_3H_8), butane (C_4H_{10}), and isobutane ($HC(CH_3)_3$) [1]. It has been found that the reaction pathway involves two H atom transfer steps with small activation energies. We have demonstrated that the synergy of two active sites, *B-O-O-B* and *B-O-B*, is crucial for the first and second H-transfer, respectively. We have demonstrated that these active sites play an important role in producing alkenes counterpart of the mentioned alkanes. The charge redistribution during H-transfers and localized oxygen atomic states in the conduction band are explored to suggest possible descriptors for the rational design of new catalysts. The universal action of the *B-O-O-B* and *B-O-B* active sites for ODH of the light alkanes paves the way for metal-free BN-based materials for future catalytic applications.

Alumina-supported nickel-based catalysts, $Ni@Al_2O_3$, constitute an important class of catalytic materials with a wide range of industrial applications, such as natural gas reforming for syngas production and oxidative dehy-

drogenation (ODH) of alkanes. When used in ODH catalysis, it has been assumed that the active species in these materials are NiO crystallites dispersed on alumina and nickel aluminate species ($NiAl_2O_4$), both with Ni in its common +2 oxidation state. These morphologies are believed to be responsible for the high selectivity of this class of catalysts as compared to unsupported pure NiO crystallites. However, more recently, the formation of a Ni^{3+} species, which promotes the isolation of electrophilic oxygen (O^-), has been invoked to explain the high selectivity for ethylene formation from ethane. The complexity and inhomogeneity of the condensed phase reaction environment often preclude a complete molecular-level understanding of the active species and underlying reaction mechanisms. Therefore, it proves helpful to study small metal oxide clusters in the gas phase. Such clusters provide atom-specific insights into the interactions governing structure-reactivity correlations at the molecular level and ultimately can serve as isolated model systems for active sites in real catalysts. Therefore, we have studied the geometric and electronic structures of $Ni_xAl_yO_z^+$ clusters to identify such model systems for $Ni@Al_2O_3$ ODH catalysts [2]. As charged clusters are required for mass selection, we have chosen mixed metal oxide cations with the composition $(NiO_m)(Al_2O_3)_n(AlO)^+$ with $m = 1-2$ and $n = 1-3$. For $m = 1$, the addition of the NiO moiety ensures formally fully oxidized clusters with all metal atoms in their

most common oxidation state (Al^{3+} and Ni^{2+}). Addition of one more O atom in the $m = 2$ series allows for the study of oxygen-rich species, which may contain less common Ni^{3+} centers in combination with O^- species such as those invoked to explain enhanced ODH selectivity.

Borophene is a collective name for two-dimensional (2D) boron sheets or crystalline atomic monolayers of boron. Typically, such sheets have to contain periodic B vacancies to maintain structural stability, and these vacancies may appear in a great variety of different motifs. This makes borophene a highly polymorphic material. A great variety of borophene structures were extensively studied in the past decade in the quest for graphene-like materials with potential for advanced applications in catalysis and technology. Among them, the 2D honeycomb boron is of specific interest as a structural analog of graphene. Recently it has been synthesized on the Al(111) substrate; however, it remains unknown to what extent does honeycomb boron behaves like graphene. Therefore, we have elucidated the structural and electronic properties of this unusual 2D material using extensive DFT calculations in order to explain recent experimental findings [3]. We have demonstrated that in contrast to graphene on lattice-mismatched metal surfaces, honeycomb boron cannot wiggle like a blanket on Al(111), but rather induces reconstruction of the top metal layer, forming a stoichiometric AlB_2 sheet on top of Al. Our conclusions from theoretical modeling are fully supported by X-ray absorption spectra showing strong similarity in the electronic structure of honeycomb boron on Al(111) and thick AlB_2 films. On the other hand, a clear separation of the electronic states of the honeycomb boron into π - and σ -subsystems indicates an essentially 2D nature of the electronic system in both one-layer AlB_2 and bulk AlB_2 . In other words, honeycomb boron essentially matched the metallic substrate aluminum's structure so closely that it could not be con-

sidered an independent, freestanding layered material.

References

- [1] S. Kumar, A. Lyalin, Z. Huang, and T. Taketsugu, *Catalytic Oxidative Dehydrogenation of Light Alkanes over Oxygen Functionalized Hexagonal Boron Nitride*, *ChemistrySelect* **7**, e202103795 (2022).
- [2] Y. Li, M. C. Babin, S. Debnath, T. Iwasa, S. Kumar, T. Taketsugu, K. R. Asmis, A. Lyalin, D. M. Neumark, *Structural Characterization of Nickel-Doped Aluminum Oxide Cations by Cryogenic Ion Trap Vibrational Spectroscopy*, *J. Phys. Chem. A* **125**, 9527-9535 (2021).
- [3] A. Preobrajenski, A. Lyalin, T. Taketsugu, N. A. Vinogradov, and A. S. Vinogradov, *Honeycomb Boron on Al(111): from the Concept of Borophene to the Two-Dimensional Boride*, *ACS Nano* **15**, 15153 – 15165 (2021).

Development of fundamental simulation code for magnetic materials

Tetsuya FUKUSHIMA

*Institute for Solid State Physics, University of Tokyo
Kashiwa-no-ha, Kashiwa, Chiba 277-8581*

This year, we have developed a fundamental simulation code for calculating the magnetic properties of permanent magnets and spintronics materials. The automatic exhaustive calculations in this study are based on the all-electron full-potential (Korringa-Kohn-Rostoker) KKR Green's function method (FP-KKR). Since the potential is anisotropic rather than spherically symmetric, we can calculate not only the magnetization and Curie temperature but also the magnetocrystalline anisotropy energy constant (K_u) with high accuracy. The KKR Green's function method can also be conveniently combined with the coherent potential approximation (CPA). It is free from using supercells, resulting in reduced computational costs drastically. Therefore, it is possible to perform efficient calculations for a huge number of compositions of disordered alloys. We have applied this calculation method to YCo_5 , SmCo_5 , and $\text{Sm}_2\text{Fe}_{17}\text{N}_3$ based alloys.

Fig. 1 shows the calculated K_u and magnetization (J_s) of $\text{Y}(\text{Co},\text{Fe},\text{Ni},\text{Cu})_5$. The addition of low concentrations of iron, nickel, and copper alone increases K_u as compared to the value of YCo_5 . On the other hand, J_s decreases at low concentrations regardless of the type of added elements. For high concentration ranges, the addition of cobalt and nickel constantly decreases the J_s . In contrast, an increase in J_s can be confirmed for the iron additions in the high concentration region; from the upper right of Fig. 1, YFe_3Co_2 can be rec-

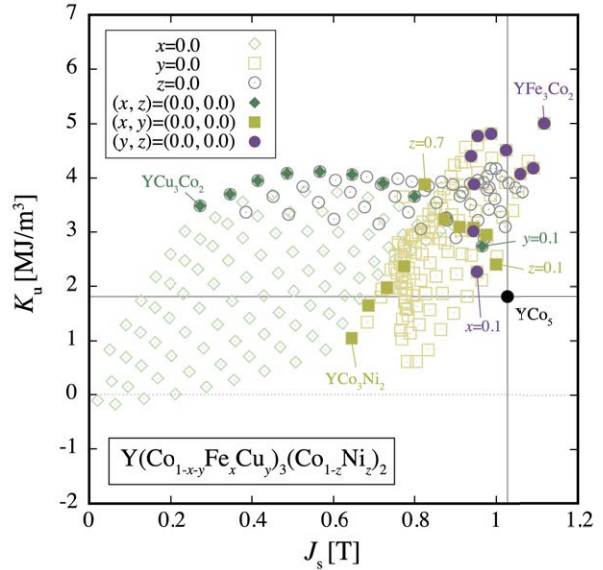


Figure 1: Calculated K_u and J_s for disordered $\text{Y}(\text{Co},\text{Fe},\text{Ni},\text{Cu})_5$.

ognized as the material with the largest K_u and J_s among calculated compositions.

In practice, the 1-5 phases cannot exist stably at high iron concentrations. In samarium systems, nickel has been added as a stabilizing element to the 1-5 phases [1]. A similar composition, $\text{YFe}_3(\text{Co}_{1-z}\text{Ni}_z)_2$, is also considered for the yttrium system. However, the performance deteriorates as a trade-off for phase stability; thus it is necessary to search for the optimum composition. In the present study, it was confirmed that up to $z \sim 0.5$, the anisotropy field is comparable to that of YCo_5 .

References

- [1] A. Landa, P. Söderlind, E. E. Moore, and A. Perron, *Appl. Sci.* **10**, 1 (2020).

Novel chloride solid electrolytes for all solid-state sodium metal battery (2)

Masanobu NAKAYAMA, Naoto TANIBATA, Ryo KOBAYASHI

Department of Advanced Ceramics,

Nagoya Institute of Technology, Gokiso-cho, Showa-ku, Nagoya, Aichi 466-8555

Since discovery of fast Li^+ conductive chloride, Li_3YCl_6 , by Asano *et al.* in 2018[1], much attention has been developed for searching high ionic conductive chlorides. In this study, we focused on search for novel Na^+ conductive chlorides in terms of “element strategy” (Japanese government policy in science and technology since 2007). Using high-throughput force field (FF) calculations, Na ion conductivities are evaluated exhaustively for chloride materials registered in the Materials Project database.[2] Total 135 compounds which contains Na and Cl (excluding H, Li, B, C, N, O, F, S, and so on) are selected from the database, and their FF potential parameters are optimized by using cuckoo search algorithm. So far, ~ 80 compounds are optimized by referring first-principles molecular dynamics (FPMD) datasets and their Na ionic conductivities are evaluated by using FF molecular dynamics (FFMD) approach. Note that FF parameter optimization and FFMD calculations were performed using NAP software.[3,4]

Figure 1 shows a typical example of radial distribution function (RDF) for a Na and Cl-

containing compound calculated by FPMD and FFMD, showing good accordance between two approaches. Hence, the optimized FF parameters are reliable. Figure 2 displays histogram of Na ion conductivity at room temperature for 86 Na-Cl containing materials. The results indicate a few samples show fast Na^+ conductivities, $> 10^{-3}$ S/cm. Currently, we are synthesizing and evaluating ionic conductivity experimentally.

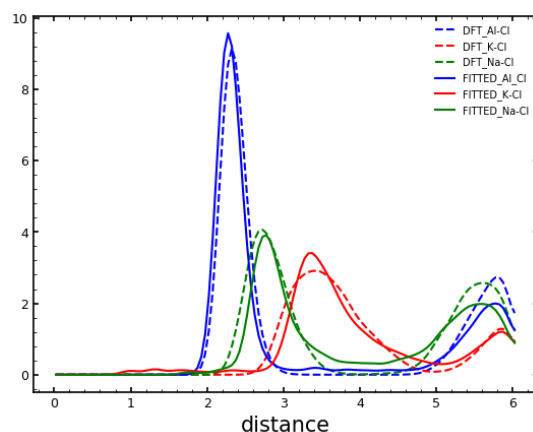


Fig. 1: Comparison between FPMD and FFMD derived RDF. FF parameters are optimized by cuckoo search algorithm.

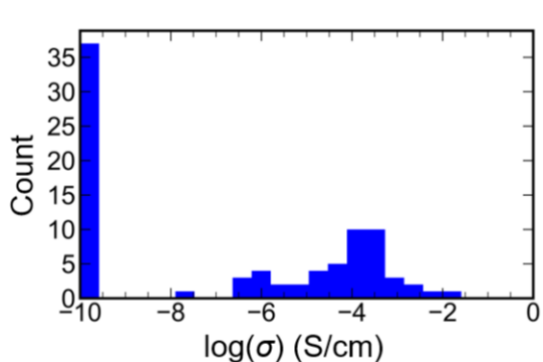


Fig. 2: Histogram of Na⁺ conductivities for Na-Cl containing materials.

References

- [1] T. Asano, A. Sakai, S. Ouchi, M. Sakaida, A. Miyazaki, S. Hasegawa, Solid Halide Electrolytes with High Lithium-Ion Conductivity for Application in 4 V Class Bulk-Type All-Solid-State Batteries, *Adv. Mater.* 30 (2018) 1803075. <https://doi.org/https://doi.org/10.1002/ama.201803075>.
- [2] A. Jain, S.P. Ong, G. Hautier, W. Chen, W.D. Richards, S. Dacek, S. Cholia, D. Gunter, D. Skinner, G. Ceder, K.A. Persson, Commentary: The Materials Project: A materials genome approach to accelerating materials innovation, *APL Mater.* 1 (2013) 11002. <https://doi.org/10.1063/1.4812323>.
- [3] R. Kobayashi, nap: A molecular dynamics package with parameter-optimization programs for classical and machine-learning potentials, *J. Open Source Softw.* 6 (2021) 2768. <https://doi.org/10.21105/joss.02768>.
- [4] R. Kobayashi, Y. Miyaji, K. Nakano, M. Nakayama, High-throughput production of force-fields for solid-state electrolyte materials, *APL Mater.* 8 (2020). <https://doi.org/10.1063/5.0015373>.

Development of high-performance permanent magnets by large-scale simulation and data-driven approach

Takashi MIYAKE

CD-FMat, AIST

Umezono, Tsukuba, Ibaraki 305-8568

Rare-earth transition-metal compounds are potential main-phase for strong permanent magnets. High content of 3d transition metals (Fe or Co) leads to high saturation magnetization, whereas rare-earth elements are essential for strong magnetocrystalline anisotropy. Because of this, structure search for Fe/Co-rich rare-earth compounds have attracted great interest. There are several known structures, such as the CaCu_5 -type structure, the $\text{Th}_2\text{Zn}_{17}$ -type structure and the ThMn_{12} -type structure. The CaCu_5 -type structure is the simplest among them, and the others are obtained by substituting transition-metal pairs (dumbbells) for rare-earth sites. There are variety of other structures obtained by different arrangement of dumbbells. In this study, we have investigated stability of these structures [1].

As a first step, we prepare a $2 \times 2 \times 2$ -supercell of SmFe_5 and SmCo_5 in the CaCu_5 -type structure, and generate hypothetical structures by replacing a part of Sm atoms with dumbbells. We compute the formation energy of all possible arrangements by density functional theory in the generalized gradient approximation. We then construct a cluster expansion model. We evaluate the formation energy of complex structures using the cluster expansion model. The result is shown in Fig.1, where the formation energies for various structures are plotted against dumbbell concentration (x). We see many structures be-

tween $x=1/3$ and $x=1/2$ whose formation energy is comparable with those of the $\text{Th}_2\text{Zn}_{17}$ - and ThMn_{12} -type structures. In contrast, the formation energy increases for $x > 1/2$.

The black solid line in the figure is the formation energy of disordered phase (so-called TbCu_7 -type structure). We compute the configuration entropy in the Bragg-Williams approximation, and evaluate the formation free energy. We found that as the temperature increases, the disordered phase is stabilized, and the solubility limits of dumbbells in SmFe_z and SmCo_z are estimated to be $z \sim 9$ at high temperature ($T=0.15$ eV).

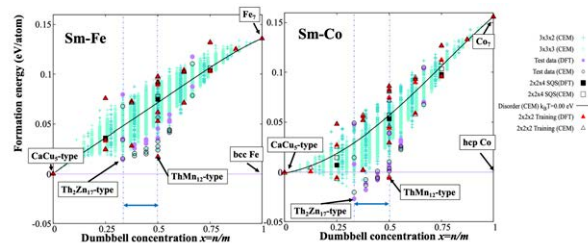


Figure 1: Formation energy of Sm-Fe and Sm-Co systems as a function of dumbbell concentrations [1].

References

- [1] Fumiaki Kuroda, Taro Fukazawa and Takashi Miyake, *Phys. Rev. Materials* **5**, 124405 (2021).

Search for the optimum interface structure with sodium ion and ion liquid on graphene using topological descriptor and machine learning

Yohei Shimizu & Hitoshi Washizu

Graduate school of simulation studies, University of Hyogo

7-1-28 Minatojima-minamimachi, Chuo-ku, Kobe, Hyogo 650-0047

1 Background and Objective

1.1 Importance of controlling the Interface of sodium ion battery

Inexpensive and large-capacity sodium-ion batteries are attracting attention as a stationary secondary power source. Ionic liquids as electrolyte is known to have the effect of increasing the diffusion of sodium ions, and optimal compounding is required.

1.2 Needs and challenges of Materials Informatics (MI)

MI predicts the properties of unknown materials from information on known materials [1] and are expected to shorten the development period. Interface MI is difficult and few previous research because of Unknown descriptor representing interface state and Infinite combinations.

1.3 Objective of our research

We establish prediction method of optimizing Interface condition of cathode sodium ion battery with physical backing using by new topological descriptor as persistent homology.

2 Simulation and Estimation method

In this research, the objective variable is the self-diffusion coefficient of sodium ion. we estimate optimizing self-diffusion coefficient condition by using results of MD simulation as teaching data. Table 1 is the method of MD simulation using LAMMPS. Considering machine learning model, we use topological descriptor as persistent homology. In general method of MI estimation model, experimental conditions such as temperature and quantity etc. is used as descriptor. The problem of these method applied to the interface simulation MI is that the search range of interface cannot be simulated infinitely and these descriptor cannot represent the physical phenomenon directly. In our previous research [2], persistent homology can express amorphous structure of polymer as persistent diagram in two dimensions based on atomic coordinates (Fig. 1). We consider persistent homology as descriptor of interface MI.

3 Results

3.1 Ability to express Interface condition using persistent homology

We compare the bulk and the interface, the diffusion coefficient in the direction parallel to the interface increased. The effect on the in-

terface is clarified by the inverse analysis of the persistent diagram. In this results, persistent diagrams can describe the state of the interface directly (Fig. 2). It can be found of the conditions for controlling the diffusion coefficient.

3.2 Prediction of self-diffusion coefficient

Regardless of the type of ionic liquid, the structure with a high diffusion coefficient shows the uniformity of the cluster. Predictions while preserving the physical meaning by directly machine learning the persistent diagram. The predictability of the interface condition using the persistent diagram as a descriptor is shown although improving accuracy is an issue (Fig. 3).

4 Conclutions

Persistent homology can express differences sodium ion and ion liquid state near graphene. Optimal interface condition can be predicted from the search range by using a persistent diagram as a descriptor.

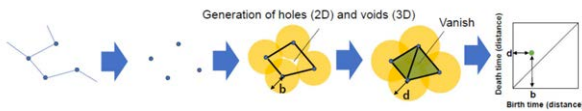


Figure 1: Principle of Persistent homology [3, 4]

Table 1: LAMMPS calculation conditions

conditions	value
Cell size	$9.12 \times 51.048 \times 20 \text{ \AA}$
Boundary condition	Periodic
Force field & Charge	Lopes' OPLS & AM1-BCC
Graphene LJ parameter	$\sigma = 0.319/nm, \epsilon = 0.392/KJ/mol$
Ion liquid quantity	$\text{Na}^+ 79 \sim 159, \text{TFSI}^- 134 \text{ or } \text{BF}_4^- 214, \text{EMI}^+ \text{ (Total charge} = 0)$
Calculation method	NVT ensemble
Temperature	250K, 300K, 350K, 400K, 450K
Time	100ns (Used to create the initial structure)

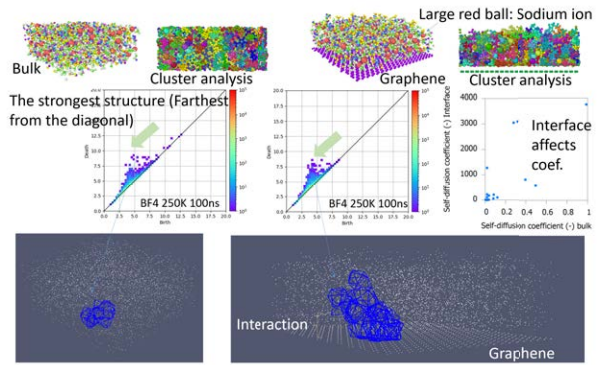


Figure 2: Difference between ion liquid bulk and interface by using persistent homology

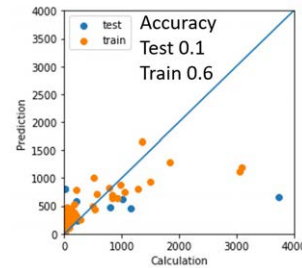


Figure 3: Prediction of the self-diffusion coefficient of sodium ion by random forest model

References

- [1] Fujimura, K., Seko, A. Tanaka, I, et al.: Adv. Energy Mater. **3** (2013) 980-985.
- [2] Shimizu, Y., Kurokawa, T., Arai, H. Washizu, H.: Sci. Rep. **11** (2021) 2274.
- [3] I.Obayashi: Siam J. Appl. Algebra Geometry **vol.2 No.4** (2018) 508-534.
- [4] http://www.wpi-aimr.tohoku.ac.jp/hiraoka_labo/homcloudenglish.html